Mode assignment of excited states in self-assembled InAs/GaAs quantum dots

Susumu Noda,* Tomoki Abe, and Masatoshi Tamura
Department of Electronic Science and Engineering, Kyoto University, Kyoto 606-8501, Japan
(Received 23 December 1997)

The modes of excited states of electrons and holes in self-assembled InAs/GaAs quantum dots (QD's) are investigated through photoluminescence (PL) and photoluminescence excitation (PLE) polarization properties with the aid of the theoretical calculation. First, the wave functions of electrons and holes are calculated by solving the three-dimensional Schrödinger equation using the finite element method by considering the effect of the strain distributions inside and/or around QD's. It is shown that there exist excited states of not only holes but also electrons in [1$\bar{1}$0] and [110] directions. Based on the results, the polarization properties of transitions between excited states of electrons and holes with the same quantum numbers are calculated. Then, the PL and PLE polarization properties are measured, and the modes of the excited states are assigned by comparing the calculation results. [S0163-1829(98)03435-3]

I. INTRODUCTION

Recently, there is much interest in self-assembled InAs/GaAs quantum dots (QD's).[1–4] The most pronounced property of the QD is in its formation of completely discrete quantum energy levels. Although there are some reports[5,6] indicating the existence of the excited states of electrons and holes through the observation of multiple peaks of photoluminescence (PL) and/or electroluminescence (EL) spectra for InAs/GaAs QD's, it has not been investigated enough (a) whether the multiple PL and/or EL peaks actually correspond to higher quantum energy levels in QD's, (b) whether any peaks are present behind the observed ones, and (c) which modes of wave functions the PL peaks correspond to. For the applications of not only interband transitions but also intersubband transitions in QD's to optoelectronic devices, it is very important to investigate the modes of the excited states of electrons and holes. Grundmann *et al.*[6] have treated the excited states in InAs/GaAs QD's where they reported that their QD's have only the ground level of electrons, and the higher-energy PL peaks are due to the transition between the ground state of electron and the excited states of holes. In this work, we have investigated the excited states of electrons and holes in self-assembled InAs/GaAs QD's through the PL and photoluminescence excitation (PLE) polarization measurements with the aid of theoretical calculation. It is shown that our QD's have the excited states of not only holes but also electrons, and the transitions between the excited states of electrons and holes with the same quantum numbers are observed, contrary to the results by Grundmann *et al.* The difference may be due to the structural differences between the individual QD's as described later. It is also found that there exist some excited states that give very weak optical emission, in addition to the ones that give the strong emission peaks. Some of the results have been briefly reported in Ref. 7. In the following we describe in detail and comprehensively the theoretical and experimental results on the excited states of the self-assembled InAs/GaAs QD's.

II. QUANTUM DOT STRUCTURE AND PHOTOLUMINESCENCE PROPERTY

The InAs/GaAs quantum dots were fabricated by Stranski-Krastanow mode molecular-beam epitaxy (MBE) growth. The growth temperature was 480 °C and the V/III ratio during the growth of the InAs dot was 8. The amount of 2 ML InAs was supplied for the dot formation. A reflection high-energy electron diffraction, a transmission electron microscope, and an atomic force microscope observations revealed that the averaged quantum dot size and structure are as shown in Fig. 1. The structure is somewhat different from that reported in Ref. 6: (a) the base lengths are much longer (25 and 30 nm) than those of Ref. 6 (12 nm), (b) the base structure of our sample has a slight unisotropy (the length of [110] is about 20% longer than that of the [1$\bar{1}$0] direction) while the sample of Ref. 6 is isotropic, and (c) the height of our QD is much lower (30 Å) than that of Ref. 6. The structural difference may be due to the slight difference in the growth conditions such as the V/III ratio, the actual growth temperature, and the growth rate. These differences in the structure strongly affect the higher quantum energy levels as described later.

Figure 2 shows the PL spectra of the sample for the various excitation levels at 13 K, where the excitation source was a multimode Ar ion laser. Many peaks appeared in

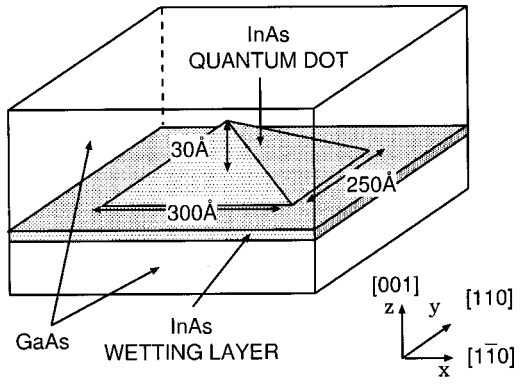

FIG. 1. Averaged quantum dot size and structure of self-assembled InAs/GaAs quantum dot investigated here.

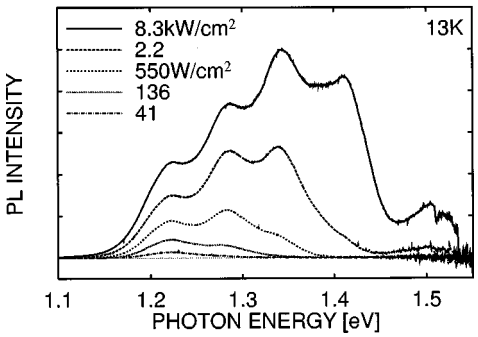

FIG. 2. PL spectra for various excitation powers at 13 K.

higher photon energy when the excitation power increased. The full width at half maximum spectral width of each peak was estimated to be 50–60 meV due to size fluctuations. In the successive sections, the following points on the PL spectra will be discussed (as described in Sec. I): (1) Do these peaks at high-excitation levels actually correspond to higher energy levels in quantum dots? (2) Are there any peaks behind the observed ones? (3) Which modes of wave functions do the PL peaks correspond to?

III. ANALYSIS OF ELECTRON AND HOLE STATES IN QD

To answer the above questions, we first calculated electron and hole envelope wave functions of the QD's by solving the Schrödinger equation using the finite element method. Although the detailed procedure of the calculation is shown in the Appendix, the essential points are summarized as follows. First of all, the strain distribution inside and/or around the QD was calculated so that the total stain energy becomes minimal using the finite element method for the QD structure shown in Fig. 1. The strain-induced changes in band gaps of InAs and GaAs, and in the band offset between them were calculated by using the strain distribution. The strain-induced modification of the electron effective mass was also calculated. On the other hand, the stain effect on the hole effective mass was not considered since the strain effect can be neglected for the first approximation. The effective mass due to heavy-hole like bands ($|\frac{3}{2},\pm\frac{3}{2}\rangle$) was utilized for holes. Strictly speaking, the mixing effect between the heavy-hole-like bands and the light-hole-like bands ($|\frac{3}{2},\pm\frac{1}{2}\rangle$) should be considered, but the mixing effect was ignored here for the following reason and/or to avoid that the calculation procedure becomes much more complicated. When we consider that our QD structure is relatively flat (which means that the lengths for the [110] and [110] directions are much longer than that of the [001] direction) and the quantum confinement effect for the [001] direction is larger than those for [110] and [110] directions, the heavy-hole-like bands are considered to have the dominant effect on the electronic properties as in a quantum-well structure.[8] Thus, the essential discussions described here are considered to hold even though we ignore the band-mixing effect. The penalty for this ignorance is that the hole mass is estimated to be slightly heavier than the actual one, and band-to-band transition wavelength is estimated to be longer than the actual one.

Then, the three-dimensional single-particle effective-mass Schrödinger equation was solved for electrons and holes, respectively, by using the finite element method. The calculated envelope wave functions for electrons and holes are shown in Figs. 3(a) and 3(b), respectively, where the distributions at the *xy* plane existing at 3 ML higher than the base plane of the pyramid were drawn. Here, *x* and *y* mean the directions of [110] and [110], respectively. The excited states are classified according to their nodes *m*, *n*, and *o* in *x*, *y*, and *z* directions, respectively, as $|m,n,o\rangle$, where *z* expresses the [001] direction. The important point in Fig. 3 is that the excited states are present for electrons in the [110] and [110]

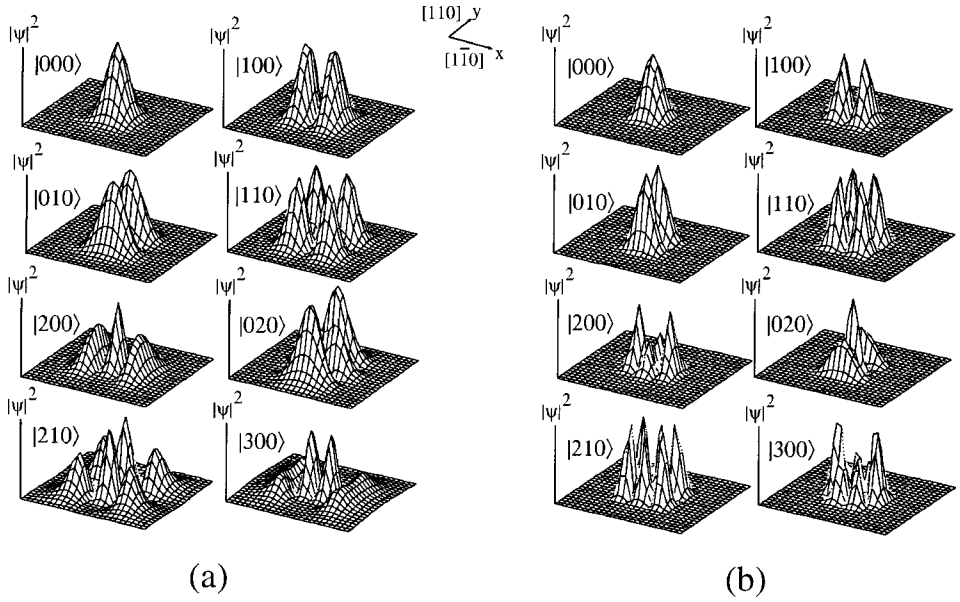

FIG. 3. Calculated envelope wave functions for (a) electrons and (b) holes, where the distributions at the *xy* plane 3 ML higher than the base plane of the pyramid were drawn. Here, *x* and *y* means the directions of [110] and [110], respectively. The excited states are classified according to their nodes *m*, *n*, and *o* in *x*, *y* and *z* directions, respectively, as $|m, n,$ and $o\rangle$, where *z* expresses [001] direction.

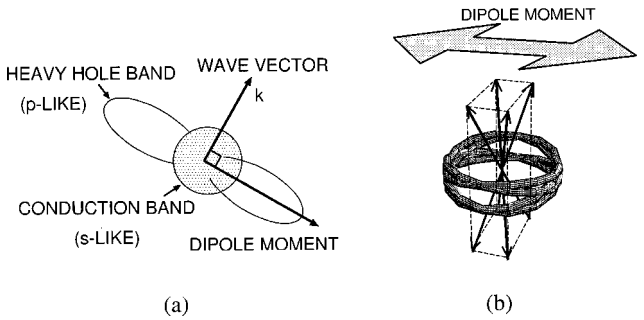

FIG. 4. (a) Bloch wave functions for each quantized wave number k, where heavy-hole-like band $|\frac{3}{2},\pm\frac{3}{2}\rangle$ is considered for holes and is rotated in the plane perpendicular to the vector k, while that of the electron is isotropic. (b) Schematic distribution of the hole Bloch wave functions for every eight wave vectors in QD.

directions, which is completely different from the result of Ref. 6. This may be due to the longer base lengths in the [110] and [110] directions in our sample. Another important point in Fig. 3 is that the excited states in the [110] and [110] directions have lower energies than that of the hole excited state in the [001] direction. This is due to the lower height in the [001] direction in our sample. Owing to these facts, the transitions between the excited states of electrons and holes in [110] and [110] directions with the same quantum numbers become possible.

IV. ANALYSIS OF POLARIZATION PROPERTIES

By utilizing the wave functions of electrons and holes obtained above, the polarization property for each transition can be theoretically calculated. The polarization property is determined with the localization of the wave functions of carriers. When electrons and holes can move around for every direction without any restriction as in bulk crystal, the wave functions for them distribute uniformly, and thus the dipole moment, which is determined by the overlap integral of the wave functions of electrons and holes, has no directional dependence. Thus, the PL spectrum has no polarization property. When the movement of electrons and holes is restricted with the introduction of the quantum structures, the wave functions tend to localize. Especially, the quantum dot structure produces the complete localization of wave functions. In this case, the envelope wave function for each energy state shown in Fig. 3 can be approximately fitted in the form of $Af_1(k_x x)f_2(k_y y)f_3(k_z z)$ by using the eight wave vectors $k=(\pm k_x, \pm k_y,$ and $\pm k_z)$ composed of specific wave numbers corresponding to the quantized energy levels in the x, y, and z directions. Here, $f_i(\ )$ expresses a sinusoidal function (sin and/or cos). For each wave vector k, the Bloch wave functions can be drawn schematically as shown in Fig. 4(a), where the heavy-hole-like band $|\frac{3}{2},\pm\frac{3}{2}\rangle$ is considered for holes as described before and is rotated in the plane perpendicular to the vector k, while that of the electron is isotropic. Figure 4(b) expresses schematically the distribution of the hole Bloch wave functions for eight wave vectors constituting one excited state in QD. As can be seen in the figure, strong localization of hole wave functions are seen, which leads to the polarization properties of the photoluminescence for each transition.

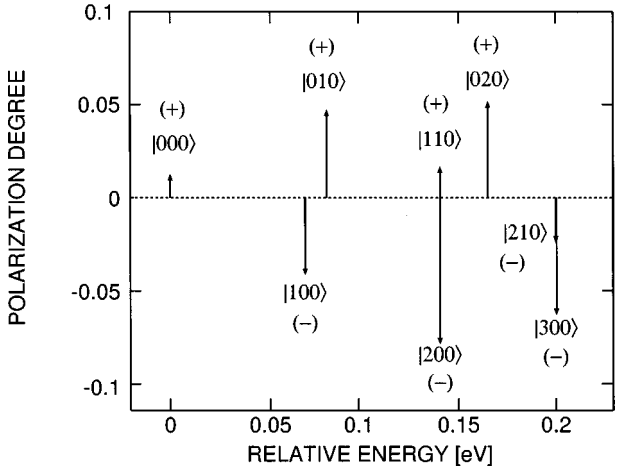

FIG. 5. Calculated polarization degree of each transition between excited states of electrons and holes with the same quantum numbers, where the polarization degree is found to become positive (+) and negative (−) according to the transition energy.

As can be seen in Fig. 4(b), the hole wave functions tend to localize for the direction with the smaller component of each wave vector k. Since the dimension of our QD's is much larger in the x,y direction compared with the z direction, the component of wave vector k becomes much smaller in the xy plane, and the hole localization occurs mainly in the xy plane. Thus, the polarization properties in the xy plane are discussed hereafter. The dipole moment matrix elements for the light polarized in the x and y directions are expressed as[9,10]

$$|M_x|^2=[\tfrac{3}{2}(k_y^2+k_z^2)/(k_x^2+k_y^2+k_z^2)]|M_{\text{bulk}}|^2, \tag{1}$$

$$|M_y|^2=[\tfrac{3}{2}(k_z^2+k_x^2)/(k_x^2+k_y^2+k_z^2)]|M_{\text{bulk}}|^2, \tag{2}$$

by using the wave numbers k_x, k_y, and k_z, and the matrix element M_{bulk} for InAs bulk crystal constituting the QD's. Here, the transitions between excited electrons and holes with the same quantum numbers are considered. The polarization degree ρ between the x and y directions in PL and/or PLE, which is defined as the ratio of the luminescence intensity between x and y directions, can be expressed by using the matrix element for each direction as

$$\rho=[|M_x|^2-|M_y|^2]/[|M_x|^2+|M_y|^2]. \tag{3}$$

$\pm k_x$, $\pm k_y$, and $\pm k_z$ can be obtained from Fig. 3 by fitting the envelope wave functions with sinusoidal functions as described above. Then the polarization properties can be calculated by using Eqs. (1)–(3). The results are shown in Fig. 5, where the polarization degree is found to become positive (+) and negative (−) according to the transition energy. Thus, the modes of the carrier wave functions corresponding to each transition can be assigned by measuring the polarization degree of PL and/or PLE spectra.

Here, we should note that the wave vector k (thus the wave numbers $\pm k_x$, $\pm k_y$, and $\pm k_z$) is determined by the carrier confinement in the quantum dots as described above, and the directions of the individual wave vectors for electrons and holes are almost equal as shown in Fig. 4(a) due to

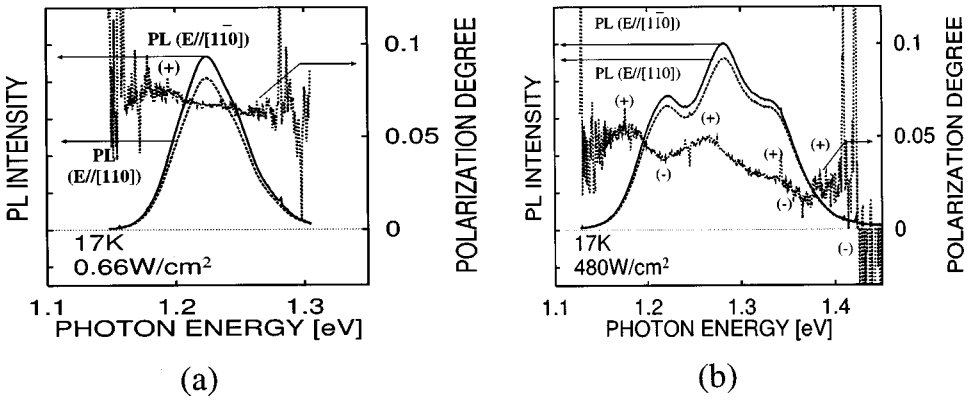

FIG. 6. PL polarization properties for low (a) and high (b) excitation powers at 13 K, where the measurement was performed for the sample with which the result of Fig. 2 was obtained.

the similar confinement effect in the quantum dots. Thus, the values of $\pm k_x$, $\pm k_y$, and $\pm k_z$ required for the calculation of Eqs. (1)–(3) can be extracted from either hole or electron wave function. Actually, the polarization properties obtained by using electron and hole wave numbers gave almost the same results. When the quantum numbers become large ($|210\rangle$ and $|300\rangle$), however, the slight difference appeared. This is probably due to the deviation of the hole wave functions from the actual ones owing to the utilization of isotropic hole mass as well as the neglect of the hole band mixing effect. To avoid the ambiguity in hole wave numbers, we have utilized the results extracted from the electron wave functions to draw Fig. 5. Since the experimental results in Fig. 6, which will be described later, show the behavior similar to the theoretical prediction, the above treatment is considered to hold.

It is also important to consider the alloy effect especially due to the In segregation effect[11] during the growth of the quantum dots. We made a calculation for the case of the In segregation length of 15 Å, and the segregation probability of 0.82 (which corresponds to the case of In segregation at growth temperature of 480 °C), where the segregation occurs mainly to the direction parallel to the growth direction (z direction). It was found that band-to-band transition energy becomes larger compared with the no-segregation case by about 40 meV. However, the polarization properties obtained almost no effect since the polarization occurs in the xy plane while the segregation effect mainly appeared in the z direction.

V. MEASUREMENT OF POLARIZATION PROPERTIES AND MODAL ASSIGNMENT

Figure 6 shows the typical PL polarization properties for (a) low- and (b) high-excitation levels at 13 K, where the measurement was performed for the sample with which the result of Fig. 2 was obtained. When the excitation level was low, the polarization degree was almost constant, and the dipole moment of the transition is considered to align mainly along the $x([1\bar{1}0])$ direction. However, when the excitation power increased, the polarization degree became smaller and larger alternately, just like the result of Fig. 5, and finally the result of Fig. 6(b) was obtained. This result indicates that the transitions between the excited electrons and holes with the modes of $|000\rangle$, $|100\rangle$, $|010\rangle$, $|110\rangle$, $|200\rangle$, $|020\rangle$, $|120\rangle$ (or $|210\rangle$) occurs. However, since individual excited states have relatively wide distributions due to the size fluctuations of the QD's, the PL emissions due to higher and lower excited states were overlapped. Thus, the polarization degree is considered to have become modified somewhat from the actual one, which leads to the shift of the peak position of the polarization spectrum. For example, the (+) polarization peak at the lowest photon energy side in Fig. 6(b) deviated from the PL peak of 1.21 eV although they are considered to be coincident with each other. Moreover, due to the overlap of the higher and lower modes emissions, the sign of the polarization degree at the higher photon energy side was strongly affected by that of the lower photon energy side owing to the band-filling effect. Thus, the negative value of ρ was difficult to observe in the PL polarization measurement. To observe the negative ρ, we have performed the PLE polarization measurement, since it gives the absorption at a specific photon energy, and the band-filling effect can be excluded. As shown in Fig. 7, the negative polarization peaks as well as the positive one have been obtained exactly, which correspond to $|200\rangle$, $|020\rangle$, and $|120\rangle$ (or $|210\rangle$). Here we should note that the peak $|120\rangle$ (or $|210\rangle$) may be overlapped with the absorption by the wetting layer.

The results obtained above are completely different from those of Grundmann *et al.*, who reported that their QD's have only the ground state of electrons, and the higher-

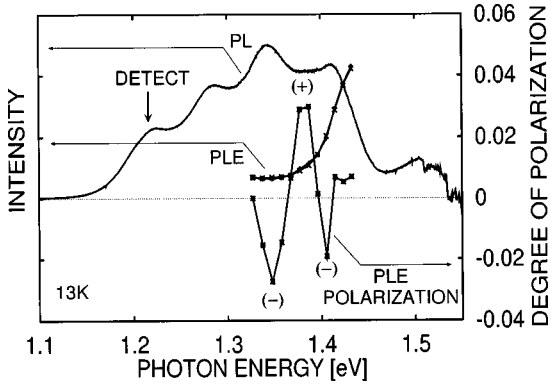

FIG. 7. PLE polarization properties.

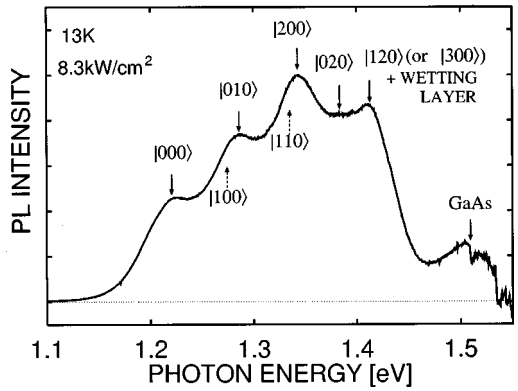

FIG. 8. Assignment of modes of higher energy levels. It is seen that the hidden peaks of $|100\rangle$ and $|110\rangle$ are present between $|000\rangle$ and $|010\rangle$ and between $|010\rangle$ and $|200\rangle$, respectively.

energy PL peaks are due to the transition between the ground state of electrons and the excited states of holes. These difference may be due to the structural difference between both QD's as described before.

Here, we assign the modes of the carrier wave functions, which give the PL spectra of Fig. 2, as Fig. 8 through the careful comparison between theoretical and experimental results. It is seen that the hidden peaks of $|100\rangle$ and $|110\rangle$ are present between $|000\rangle$ and $|010\rangle$ and between $|010\rangle$ and $|200\rangle$, respectively. The weak emission of $|100\rangle$ may be due to the strong phonon interaction, but the detail is under consideration.

VI. CONCLUSION

We have assigned the modes of excited states of electrons and holes in self-assembled InAs/GaAs QD's by investigating PL and PLE polarization properties with the aid of the theoretical calculation. First of all, the wave functions of electrons and holes have been calculated by solving the three-dimensional Schrödinger equation using the finite element method by considering the effect of the strain distributions inside and/or around QD's. It has been shown that there exist excited states of not only holes but also electrons in [110] and [110] directions in our QD's. Based on the results, the polarization properties of transitions between excited states of electrons and holes with the same quantum numbers have been calculated. Then, the PL and PLE polarization properties were measured, and the modes of the excited states were assigned by comparing the calculation results. It has been shown that some hidden peaks are present between apparent peaks, respectively. The weak emission of the hidden peaks may be due to the strong phonon interaction.

ACKNOWLEDGMENTS

The authors would like to thank Professor A. Sasaki and Dr. A. Wakahara for fruitful discussions. This work was supported in part by a Grant-in-Aid from the Ministry of Education, Science, Sports, and Culture of Japan.

APPENDIX: DETAILED PROCEDURE OF CALCULATION FOR ENVELOPE WAVE FUNCTIONS

First, the strain distribution inside and/or around the QD was calculated so that the total stain energy U becomes minimal using the finite element method for the QD structure shown in Fig. 1.

The strain energy U is expressed as

$$U=\tfrac{1}{2}\int\int\int \sigma^t(\varepsilon-\varepsilon_0)dx\ dy\ dz, \tag{A1}$$

where ε is the strain vector, σ is the stress vector, and ε_0 is the initial strain vector.[12] ε is expressed by using the displacements u, v, w in the x, y, and z directions, respectively, as

$$\varepsilon=\begin{pmatrix}\varepsilon_{xx}\\ \varepsilon_{yy}\\ \varepsilon_{zz}\\ \varepsilon_{xy}\\ \varepsilon_{yz}\\ \varepsilon_{zx}\end{pmatrix}=\begin{pmatrix}\partial u/\partial x\\ \partial v/\partial y\\ \partial w/\partial z\\ (\partial u/\partial y+\partial v/\partial x)/2\\ (\partial v/\partial z+\partial w/\partial y)/2\\ (\partial w/\partial x+\partial u/\partial z)/2\end{pmatrix}, \tag{A2}$$

where ε_{xx}, ε_{yy}, and ε_{zz} are the direct strains in the x, y, and z directions, respectively, and ε_{xy}, ε_{yz}, and ε_{zx} are the shear strains in the xy, yz, and zx planes, respectively. σ is composed of the stresses σ_{xx}, σ_{yy}, and σ_{zz} in the x, y, and z directions, respectively, and the shear stresses σ_{xy}, σ_{yz}, and σ_{zx} in the xy, yz, and xz planes, respectively, and expressed as

$$\sigma=\begin{pmatrix}\sigma_{xx}\\ \sigma_{yy}\\ \sigma_{zz}\\ \sigma_{xy}\\ \sigma_{yz}\\ \sigma_{zx}\end{pmatrix}=D(\varepsilon-\varepsilon_0)+\sigma_0,$$

$$D=\begin{pmatrix}C_{11}&C_{12}&C_{12}&0&0&0\\ C_{12}&C_{11}&C_{12}&0&0&0\\ C_{12}&C_{12}&C_{11}&0&0&0\\ 0&0&0&C_{44}&0&0\\ 0&0&0&0&C_{44}&0\\ 0&0&0&0&0&C_{44}\end{pmatrix}. \tag{A3}$$

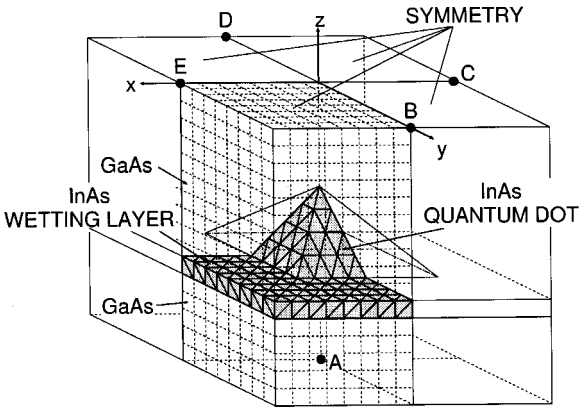

FIG. 9. Schematic to show the division of voxels for the finite element method.

σ_0 is the initial stress, D is the matrix composed of elastic constants C_{11}, C_{12}, and C_{44}, which combines the strain with the stress.

The quantum dot is divided as shown in Fig. 9, where each voxel has 15 Å, 12.5 Å, and 3 Å, for the x, y, and z directions, respectively. The displacements (u, v, and w) at each node of voxel (x,y,z) were first calculated so that the strain energy U becomes minimal. The displacements at any point of the voxel were estimated by the linear interpolation using the values of each node. Then, the strain distribution inside and/or around the quantum dot can be obtained from u, v, and w, obtained. In the calculation, the initial stress σ_0 was set to be zero, and the initial strain ε_0 was given for InAs as $\varepsilon_{xx0}=\varepsilon_{yy0}=\varepsilon_{zz0}=(a_{\mathrm{InAs}}-a_{\mathrm{GaAs}})/a_{\mathrm{GaAs}}$ where a_{InAs} and a_{GaAs} are lattice constants of InAs and GaAs, respectively, without strain. The boundary conditions were as follows: (i) the displacements at the base plane (the xy plane that passes through the point A in Fig. 9) are zero, and (ii) the periodic boundary conditions are employed, and the displacements at the edge planes (the xz plane that passes through points B and D, and the yz plane that passes through points C and E in Fig. 9) are zero.

Then, the strain-induced changes in the band offset between InAs and GaAs were calculated by using the strain distribution obtained above. The energy changes of heavy-hole (ΔE_{HH}), light-hole (ΔE_{LH}), and spin split-off bands (ΔE_{SO}) can be obtained from the kp perturbation theory,[13,14] where the perturbation Hamiltonian is expressed as

$$H_\varepsilon=\begin{array}{c}\begin{array}{cccccc}\left|\frac{3}{2},\frac{3}{2}\right\rangle & \left|\frac{3}{2},\frac{1}{2}\right\rangle & \left|\frac{3}{2},-\frac{1}{2}\right\rangle & \left|\frac{3}{2},-\frac{3}{2}\right\rangle & \left|\frac{1}{2},\frac{1}{2}\right\rangle & \left|\frac{1}{2},-\frac{1}{2}\right\rangle\end{array}\\ \begin{pmatrix} P_\varepsilon+Q_\varepsilon & -S_\varepsilon & R_\varepsilon & 0 & 1/2^{1/2}S_\varepsilon & -2^{1/2}R_\varepsilon \\ -S_\varepsilon^* & P_\varepsilon-Q_\varepsilon & 0 & R_\varepsilon & 2^{1/2}Q_\varepsilon & -(\frac{3}{2})^{1/2}S_\varepsilon \\ R_\varepsilon^* & 0 & P_\varepsilon-Q_\varepsilon & S_\varepsilon & -(\frac{3}{2})^{1/2}S_\varepsilon^* & -2^{1/2}Q_\varepsilon \\ 0 & R_\varepsilon^* & S_\varepsilon^* & P_\varepsilon+Q_\varepsilon & 2^{1/2}R_\varepsilon^* & 1/2^{1/2}S_\varepsilon^* \\ 1/2^{1/2}S_\varepsilon^* & 2^{1/2}Q_\varepsilon & -(\frac{3}{2})^{1/2}S_\varepsilon & 2^{1/2}R_\varepsilon & P_\varepsilon+\Delta_0 & 0 \\ -2^{1/2}R_\varepsilon^* & -(\frac{3}{2})^{1/2}S_\varepsilon^* & -2^{1/2}Q_\varepsilon & 1/2^{1/2}S_\varepsilon & 0 & P_\varepsilon+\Delta_0 \end{pmatrix}\end{array}, \tag{A4}$$

where

$$\begin{aligned} P_\varepsilon &= a_s(\varepsilon_{xx}+\varepsilon_{yy}+\varepsilon_{zz}),\\ Q_\varepsilon &= b_s/2(2\varepsilon_{zz}-\varepsilon_{xx}-\varepsilon_{yy}),\\ S_\varepsilon &= -d_s(\varepsilon_{zx}-i\varepsilon_{yz}),\\ R_\varepsilon &= 3^{1/2}b_s/2(\varepsilon_{xx}-\varepsilon_{yy})-id_s\varepsilon_{xy}, \end{aligned} \tag{A5}$$

and a_s, b_s, and d_s are constants that express hydrostatic, uniaxial, and shear components.

Since it was found from the strain calculations described above that the shear strains (ε_{xy}, ε_{yz}, and ε_{zx}) and the differences between individual direct strains (ε_{xx}, ε_{yy}, and ε_{zz}) are very small, the values of S_ε and R_ε become very small, and therefore the above Hamiltonian can be easily solved. In this case, the eigenvalues, that is ΔE_{HH}, ΔE_{LH}, and ΔE_{SO} are expressed as

$$\begin{aligned} \Delta E_{\mathrm{HH}} &= -P_\varepsilon-Q_\varepsilon,\\ \Delta E_{\mathrm{LH}} &= -P_\varepsilon+1/2\{Q_\varepsilon-\Delta_0+(\Delta_0^2+2\Delta_0Q_\varepsilon+9Q_\varepsilon^2)^{1/2}\},\\ \Delta E_{\mathrm{SO}} &= -P_\varepsilon+1/2\{Q_\varepsilon-\Delta_0-(\Delta_0^2+2\Delta_0Q_\varepsilon+9Q_\varepsilon^2)^{1/2}\}. \end{aligned} \tag{A6}$$

On the other hand, the strain-induced energy shift in conduction band ΔE_C is expressed as

$$\Delta E_C=P_\varepsilon=a_s(\varepsilon_{xx}+\varepsilon_{yy}+\varepsilon_{zz}), \tag{A7}$$

which depends only on the hydrostatic component of the strain. By using Eqs. (A6) and (A7), the strain-induced changes ΔE_C, ΔE_{HH}, ΔE_{LH}, and ΔE_{SO} can be obtained. These values were added to the InAs/GaAs band offsets without strain for a deduction of the electron and hole confinement potentials under strain. The band offset ratio for the unstrained bands is taken from the difference in absolute energetic position of the average valence band $E_{v,\mathrm{av}}$.[13]

The strain-induced modification of the electron effective mass was also considered, and it is expressed as[15]

TABLE I. Numerical parameters utilized for the calculations.

	InAs	GaAs
a_0 (Å)	6.0584	5.6532
C_{11} (10^{11} dyn/cm^3)	8.329	11.88
C_{12} (10^{11} dyn/cm^3)	4.562	5.38
a_s (eV)	−1.0	−1.16
b_s (eV)	−1/8	−1.7
d_s (eV)	−3.6	−4.5
a_c (eV)	−5.08	−7.17
Δ_0 (eV)	0.38	0.34
$E_{v,\mathrm{av}}$ (eV)	−6.67	−6.92
E_g (eV)	0.359	1.435
m_e (m_0)	0.027	0.068
m_{HH} (m_0)	0.41	0.5

$$1/m_{\parallel}^{*}=1/m_0+P^2/3[3/E_{g\mathrm{HH}}+(\alpha-2^{1/2}\beta)^2/E_{g\mathrm{LH}}+(\beta+2^{1/2}\alpha)^2/E_{g\mathrm{SO}}],$$
$$1/m_{\perp}^{*}=1/m_0+2P^2/3[(2^{1/2}\alpha-\beta)^2/E_{g\mathrm{LH}}+(2^{1/2}\beta+\alpha)^2/E_{g\mathrm{SO}}], \quad \text{(A8)}$$

where P is the momentum matrix element of the interband transition. $E_{g\mathrm{HH}}$, $E_{g\mathrm{LH}}$, and $E_{g\mathrm{SO}}$ are the energy gaps between the conduction band and the heavy-hole (HH), light-hole (LH), and spin-orbit (SO) bands, respectively, under the strain. $\parallel$ and $\perp$ express the parallel and perpendicular directions to the substrate surface, respectively. The elements α and β are dimensionless parameters representing the strain-induced mixing between the LH and the SO split band, and are expressed as

$$\alpha=8^{1/2}|Q_\varepsilon|/C,$$
$$\beta=(A-B)|Q_\varepsilon|/(CQ_\varepsilon), \quad \text{(A9)}$$

where $A=\Delta_0+Q_\varepsilon$, $B=(\Delta_0^2+2\Delta_0 Q_\varepsilon+9Q_\varepsilon^2)^{1/2}$, and $C=[2B(B-A)]^{1/2}$.

Then, the three-dimensional single-particle effective-mass Schrödinger equation was solved for electrons and holes, respectively, by using the finite element method. The Hamiltonian is as follows:

$$H_i=-(h/2\pi)^2/\{2m_i^{*}(x,y,z)\}\nabla^2+V_i(x,y,z), \quad \text{(A10)}$$

where i equals c, HH, and LH and expresses the conduction, heavy-hole, and light-hole bands, respectively. In the case of the conduction band, m_c^{*} becomes tensor, which components are expressed by Eq. (A8). $V_i(x,y,z)$ can be obtained by using Eqs. (A6) and (A7) as described above. The excitonic effect was ignored here since our quantum dot is in the strong confinement regime, and the size quantization represents the dominant part of the carrier energy.

The numerical values utilized for the calculation are listed in Table I. The resultant envelope functions for electrons and holes are shown in Fig. 3.

*Electronic address: snoda@kuee.kyoto-u.ac.jp

[1] M. Tabuchi, S. Noda, and A. Sasaki, in *Science and Technology of Mesoscopic Structures*, edited by S. Namba, C. Hamaguchi, and T. Ando (Springer, Tokyo, 1992), p. 379.

[2] D. Leonard, M. Krishnamurty, C. M. Reaves, S. P. DenBaars, and P. M. Petroff, Appl. Phys. Lett. **63**, 3203 (1993).

[3] Y. Nabetani, T. Ishikawa, S. Noda, and A. Sasaki, J. Appl. Phys. **76**, 347 (1994).

[4] M. Grundmann, O. Stier, and D. Bimberg, Phys. Rev. B **52**, 11 969 (1995).

[5] P. M. Petroff and S. P. DenBaars, Superlattices Microstruct. **15**, 15 (1994).

[6] M. Grundmann, N. N. Ledentsov, O. Stier, and D. Bimberg, Appl. Phys. Lett. **68**, 979 (1996).

[7] S. Noda, T. Abe, M. Tamura, and A. Sasaki, *8th Conference on Modulated Semiconductor Structure (MSS8), Santa Barbara, 1997*, special issue of Physica E (to be published).

[8] M. A. Cusack, P. R. Briddon, and M. Jaros, Phys. Rev. B **54**, R2300 (1996); **56**, 4047 (1997).

[9] E. O. Kane, J. Phys. Chem. Solids **1**, 249 (1957).

[10] Y. Miyamoto, Y. Miyake, M. Asada, and Y. Suematsu, IEEE J. Quantum Electron. **25**, 2001 (1989).

[11] H. Yamaguchi and Y. Horikoshi, J. Appl. Phys. **68**, 1610 (1990).

[12] O. C. Zienkiewicz, *The Finite Element Method in Engineering Science* (McGraw-Hill, New York, 1971).

[13] Chris G. Van de Walle, Phys. Rev. B **39**, 1871 (1989).

[14] M. Sugawara, N. Okazaki, T. Fujii, and S. Yamazaki, Phys. Rev. B **48**, 8102 (1993).

[15] F. H. Pollak, *Semiconductors and Semimetals* (Academic, New York, 1991), Vol. 33, Chap. 2.